On the Theory of Discrete TLM Green's Functions in Three-Dimensional TLM

Michael Krumpholz, *Member, IEEE,* Bernhard Bader, *Student Member, IEEE,* and Peter Russer, *Fellow, IEEE*

***Abstract*—The response to a wave pulse incident on the boundary of a certain spatial domain may be represented by discrete TLM Green's functions. On the other hand, the response to a localized electromagnetic excitation at the boundary of a certain spatial domain may be calculated directly from Maxwell's equations and be represented by analytic TLM Green's functions. For low frequencies and small wave numbers, the analytic TLM Green's functions coincide with the discrete TLM Green's functions. Applying the analytic TLM Green's functions in the absorbing boundary condition at the boundary to the open half-space reduces the computational effort considerably when compared with the application of the discrete TLM Green's functions.**

I. Introduction

ORIGINALLY, the TLM-method was based on the analogy of the propagation of an electromagnetic wave in space with the signal propagation in a mesh of transmission lines [1]–[3]. Recently, derivations of the three-dimensional TLM-method with condensed symmetric node [4] from Maxwell's equations have been given [5]–[8]. The discrete TLM Green's functions [9] are defined as the response to a single wave pulse excitation. Due to the field theoretic foundation of the TLM method, there should be a relation between the discrete TLM Green's functions and the response to a localized electromagnetic excitation calculated directly from Maxwell's equations. In the following, we use the term *analytic TLM Green's functions* for the discretized response to a localized electromagnetic excitation. The objective of this paper is to demonstrate the relation between the discrete TLM Green's functions and the analytic TLM Green's functions as well as the advantages connected with the use of the analytic TLM Green's functions.

The response to a wave pulse incident on the boundary of a certain spatial domain is nonlocal with respect to space and time. This response may be represented by discrete TLM Green's functions describing the relation between the wave pulses incident on the boundary and the wave pulses scattered from the boundary of the spatial domain. In this paper, we restrict ourselves to discrete TLM Green's functions describing the response to an excitation in the boundary surface separating homogeneous spatial domains. This type of discrete Green's function is highly attractive since it allows one to analyze a structure by partitioning it in substructures. This method is known as time domain diakoptics [10].

As an example, we consider the discrete Green's functions for the open half-space allowing us to model the absorbing boundary condition at the boundary to the open half-space. We calculate the analytic TLM Green's functions directly from Maxwell's equations by discretizing the response to a localized electromagnetic excitation at the boundary of open half-space. The analytic TLM Green's functions and the discrete TLM Green's functions are identical for low frequencies and small wave numbers. This is shown by assuming a Gaussian excitation of the open half-space instead of a single wave pulse and by filtering the discrete TLM Green's function in spectral domain. The filtering in spectral domain is necessary, because the discrete TLM Green's functions consist of parts describing physical modes with small wave numbers as well as spurious modes with large wave numbers, which both contribute to frequencies approaching to zero [11]–[13].

The absorbing boundary condition at the boundary of the open half-space is modelled by convolving the wave pulses incident on the boundary to the open half-space with the discrete TLM Green's functions and the analytic TLM Green's functions, respectively. The analytic TLM Green's functions represent the discretized response to an excitation corresponding to a single TLM wave pulse at the boundary. Analytically, the spatial distribution of this excitation is represented by a two-dimensional delta, pulse, and triangle function. The response to this excitation is given by a spherical wave reflected from the boundary. This spherical wave is bounded close around a sphere with the radius $r = ct$, where c is the free space velocity of light. Thus the convolution may be restricted to a set of pulses in a neighbourhood of this sphere. This property allows one to reduce the convolution by one dimension and to reduce the convolution in two-dimensional space and time to a convolution in two-dimensional space, respectively. The absorbing boundary condition is applied in the simulation of a short-circuited microstrip line. The TLM results are compared with the results obtained by analyzing the same microwave structure with the FDTD method.

II. The Discrete TLM Green's Functions

We consider discrete TLM Green's functions describing the relation between the wave pulses incident on the boundary

Manuscript received August 19, 1994; revised December 14, 1994. This work was supported by the Deutsche Forschungsgemeinschaft (DFG), Bonn, Germany.

M. Krumpholz was at the Ferdinand-Braun-Institut für Höchstfrequenztechnik, Berlin, Germany. He is now with Radiation Laboratory EECS, University of Michigan, Ann Arbor, MI USA.

B. Bader is with Ferdinand-Braun-Institut für Höchstfrequenztechnik, Berlin, Germany.

P. Russer is with Ferdinand-Braun-Institut für Höchstfrequenztechnik, Berlin, Germany, and Lehrstuhl für Hochfrequenztechnik, Technische Universität, München, Germany.

IEEE Log Number 9412036.

and the wave pulses scattered from the boundary of the spatial domain. This relation is given by the convolution

$$ {}_k\boldsymbol{b}_n = {}_k\boldsymbol{G}_n *_k \boldsymbol{a}_n = \sum_{n',k'=-\infty}^{\infty} {}_{k-k'}\boldsymbol{G}_{n,n'} \; {}_{k'}\boldsymbol{a}_{n'} \tag{1} $$

with

$$ \boldsymbol{n} \in B, \tag{2} $$

where

$$ B = \{n_1, n_2, \cdots, n_N\} \tag{3} $$

represents a set of N boundary nodes. The vector ${}_k\boldsymbol{a}_n$ is the column vector representing the wave pulses incident on the boundary, the vector ${}_k\boldsymbol{b}_n$ is the column vector representing the wave pulses scattered from the boundary. The matrix of the discrete Green's functions ${}_k\boldsymbol{G}_n$ describes the response to an excitation in an arbitrary boundary surface represented by N boundary nodes. The left index k denotes the discrete time coordinate related to the time coordinate t via $t = k\Delta t$.

The boundary to the open half-space at $x = 0$ is intersected by the two ports 1 and 3 of the condensed symmetric TLM node representing horizontal and vertical polarization (Fig. 1). We have used the node numbering scheme corresponding to the symmetrical representation of the scattering matrix [6], [7]. For the open half-space, four discrete TLM Green's functions are defined. The discrete TLM Green's function G^{11} describes the impulse response at port 1 of all boundary nodes due to an incident wave pulse into port 1 of one boundary node. We define the discrete TLM Green's function G^{31} as the impulse response in port 3 of all boundary nodes due to an incident wave pulse into port 1 of one boundary node. In the same way, we define the discrete TLM Green's functions G^{33} and G^{13}. With these definitions, (1) yields

$$ {}_k\begin{bmatrix} b_1 \\ b_3 \end{bmatrix}_{0,m,n} = {}_{k-k'}\begin{bmatrix} G^{11} & G^{13} \\ G_{31} & G^{33} \end{bmatrix}_{m-m',n-n'} * {}_{k'}\begin{bmatrix} a_1 \\ a_3 \end{bmatrix}_{0,m',n'}, \tag{4} $$

and

$$ \begin{aligned} {}_k[b_1]_{0,m,n} &= \sum_{m',n',k'=-\infty}^{\infty} {}_{k-k'}G^{11}_{m-m',n-n'} \; {}_{k'}[a_3]_{0,m',n'}, \\ &\quad + \sum_{m',n',k'=-\infty}^{\infty} {}_{k-k'}G^{31}_{m-m',n-n'} \; {}_{k'}[a_3]_{0,m',n'}, \\ {}_k[b_3]_{0,m,n} &= \sum_{m',n',k'=-\infty}^{\infty} {}_{k-k'}G^{13}_{m-m',n-n'} \; {}_{k'}[a_3]_{0,m',n'} \\ &\quad + \sum_{m',n',k'=-\infty}^{\infty} {}_{k-k'}G^{33}_{m-m',n-n'} \; {}_{k'}[a_3]_{0,m',n'} \end{aligned} \tag{5} $$

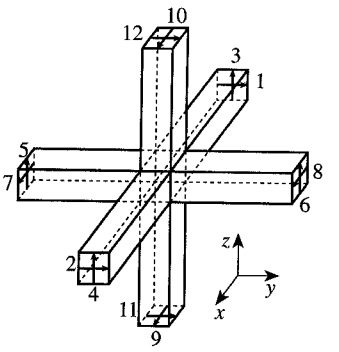

Fig. 1. A three-dimensional condensed symmetric TLM node.

respectively. The discrete space coordinates in y- and z-direction are related to the space coordinates via $y = m\Delta l$ and $z = n\Delta l$. The discrete space coordinate l related to the x-coordinate via $x = l\Delta l$ is zero at the boundary to the open half-space.

The functions G^{11} and G^{31} may be calculated numerically or algebraically [14], [15]. G^{33} and G^{13} are obtained by a positive 90°-rotation of G^{11} and G^{31} around the x-axis. According to Fig. 1, we obtain

$$ {}_kG^{33}_{m,n} = {}_k\,G^{11}_{m,n}|_{90°}, \tag{6} $$

since by a positive 90°-rotation around the x-axis, a_1 is transformed into a_3, and

$$ {}_kG^{13}_{m,n} = -{}_kG^{31}_{m,n}|_{90°} \tag{7} $$

because by the same 90°-rotation, a_3 is transformed into $-a_1$. A positive 90°-rotation of a function $f(m,n)$ is described by the transition $f(m,n) \rightarrow f(n,-m)$. Using the symmetries [14] ${}_kG^{11}_{n,-m} = -{}_kG^{11}_{m,n}$ and ${}_kG^{31}_{n,-m} = -{}_kG^{31}_{m,n}$ yields the symmetry relations

$$ {}_kG^{33}_{m,n} = -{}_kG^{11}_{m,n} \tag{8} $$

and

$$ {}_kG^{13}_{m,n} = {}_kG^{31}_{m,n}. \tag{9} $$

III. The Analytic TLM Green's Functions

For the calculatation of the analytic TLM Green's functions for the open half-space given by $x \geq 0$, we start with the wave equation

$$ \Delta\boldsymbol{F} - \frac{1}{c^2}\frac{\partial^2 \boldsymbol{F}}{\partial t^2} = 0 \tag{10} $$

where $\boldsymbol{F}$ represents the electric or the magnetic field vector, $\boldsymbol{F} = \boldsymbol{E}, \boldsymbol{H}$. We transform the wave equation into spectral domain with respect to the coordinates t, y, and z. The Fourier transformation with respect to the time variable t and the space

$$ \begin{aligned} \overline{\boldsymbol{F}}(x, k_y, k_z, \omega) &= \mathcal{F}\{\boldsymbol{F}(x,y,z,t)\} \\ &\cdot \equiv \int_{-\infty}^{+\infty}\int_{-\infty}^{+\infty}\int_{-\infty}^{+\infty} \boldsymbol{F}(x,y,z,t) e^{-\jmath(k_y y + k_z z + \omega t)} \, dy \, dz \, dt \end{aligned} \tag{11} $$

variables y and z is defined by (11) as shown at the bottom of the preceding page, and

$$\begin{aligned}\boldsymbol{F}(x,y,z,t) &= \mathcal{F}^{-1}\{\overline{\boldsymbol{F}}(x,k_y,k_z,\omega)\} \\ &\equiv \frac{1}{8\pi^3}\int_{-\infty}^{+\infty}\int_{-\infty}^{+\infty}\int_{-\infty}^{+\infty} \\ &\quad \cdot \overline{\boldsymbol{F}}(x,k_y,k_z,\omega)e^{\jmath(k_y y+k_z z+\omega t)}\,dk_y\,dk_z\,d\omega\end{aligned} \tag{12}$$

with the angular frequency $\omega = 2\pi f$ and the wave vector components k_y and k_z. Applying the Fourier transformation to (10), we obtain

$$\frac{\partial^2\overline{\boldsymbol{F}}(x,k_y,k_z,\omega)}{\partial x^2} - \left(k_y^2+k_z^2-\frac{\omega^2}{c^2}\right)\overline{\boldsymbol{F}}(x,k_y,k_z,\omega) = 0. \tag{13}$$

Separating this equation into cartesian components $\overline{F}_\mu$ with $\mu = x,y,z$ yields

$$\frac{\partial^2\overline{F}_\mu(x,k_y,k_z,\omega)}{\partial x^2} - \left(k_y^2+k_z^2-\frac{\omega^2}{c^2}\right)\overline{F}_\mu(x,k_y,k_z,\omega) = 0. \tag{14}$$

We solve (14) for the open half-space given by $x \geq 0$ considering the initial value problem with respect to the x-coordinate. We use the Laplace transformation

$$\begin{aligned}\tilde{F}_\mu(p,k_y,k_z,\omega) &= \mathcal{L}\{\overline{F}_\mu(x,k_y,k_z,\omega)\} \\ &\equiv \int_0^\infty \overline{F}_\mu(x,k_y,k_z,\omega)e^{-px}\,dx\end{aligned} \tag{15}$$

and

$$\begin{aligned}\overline{F}_\mu(x,k_y,k_z,\omega) &= \mathcal{L}^{-1}\{\tilde{F}_\mu(p,k_y,k_z,\omega)\} \\ &\equiv \frac{1}{2\pi\jmath}\oint_C \tilde{F}_\mu(p,k_y,k_z,\omega)e^{px}\,dp\end{aligned} \tag{16}$$

where C represents a closed path of integration in the complex p-plane. With

$$\begin{aligned}&\mathcal{L}\left\{\frac{\partial^2\overline{F}_\mu(x,k_y,k_z,\omega)}{\partial x^2}\right\} \\ &\quad = p^2\tilde{F}_\mu(p,k_y,k_z,\omega) - p\overline{F}_\mu(x,k_y,k_z,\omega)|_{x=0} \\ &\qquad - \left.\frac{\partial\overline{F}_\mu(x,k_y,k_z,\omega)}{\partial x}\right|_{x=0}\end{aligned} \tag{17}$$

we obtain the transformed wave equation

$$\begin{aligned}&p^2\tilde{F}_\mu(p,k_y,k_z,\omega) - p\overline{F}_\mu(x,k_y,k_z,\omega)|_{x=0} \\ &\qquad - \left.\frac{\partial\overline{F}_\mu(x,k_y,k_z,\omega)}{\partial x}\right|_{x=0} \\ &\qquad - \left(k_y^2+k_z^2-\frac{\omega^2}{c^2}\right)\tilde{F}_\mu(p,k_y,k_z,\omega) = 0\end{aligned} \tag{18}$$

and

$$\begin{aligned}&\tilde{F}_\mu(p,k_y,k_z,\omega) \\ &\quad = \frac{p\overline{F}_\mu(x,k_y,k_z,\omega)|_{x=0} + \left.\dfrac{\partial\overline{F}_\mu(x,k_y,k_z,\omega)}{\partial x}\right|_{x=0}}{p^2-\left(k_y^2+k_z^2-\dfrac{\omega^2}{c^2}\right)}\end{aligned} \tag{19}$$

respectively. For $k_y^2 + k_z^2 > (\omega/c)^2$, we introduce $\alpha_1 = \sqrt{k_y^2+k_z^2-(\omega/c)^2}$. In this case, we use [16]

$$\mathcal{L}^{-1}\left\{\frac{p}{p^2-\alpha_1^2}\right\} = \cosh\alpha_1 x \tag{20}$$

and

$$\mathcal{L}^{-1}\left\{\frac{\alpha_1}{p^2-\alpha_1^2}\right\} = \sinh\alpha_1 x \tag{21}$$

for $x \geq 0$ and obtain

$$\begin{aligned}\overline{F}_\mu(x,k_y,k_z,\omega) &= \frac{e^{\alpha_1 x}}{2}\left(\overline{F}_\mu(x,k_y,k_z,\omega)|_{x=0}\right. \\ &\quad \left. + \frac{1}{\alpha_1}\left.\frac{\partial\overline{F}_\mu(x,k_y,k_z,\omega)}{\partial x}\right|_{x=0}\right) \\ &\quad + \frac{e^{-\alpha_1 x}}{2}\left(\overline{F}_\mu(x,k_y,k_z,\omega)|_{x=0}\right. \\ &\quad \left. - \frac{1}{\alpha_1}\left.\frac{\partial\overline{F}_\mu(x,k_y,k_z,\omega)}{\partial x}\right|_{x=0}\right).\end{aligned} \tag{22}$$

The function $\overline{F}_\mu(x,k_y,k_z,\omega)$ exhibits exponentially increasing and exponentially decreasing parts for increasing argument x. Since $\overline{F}_\mu(x,k_y,k_z,\omega)$ has to vanish for $x \to \infty$, (22) yields

$$\overline{F}_\mu(x,k_y,k_z,\omega)|_{x=0} = -\frac{1}{\alpha_1}\left.\frac{\partial\overline{F}_\mu(x,k_y,k_z,\omega)}{\partial x}\right|_{x=0} \tag{23}$$

which we may rewrite as

$$\left(\frac{\partial}{\partial x}+\sqrt{k_y^2+k_z^2-(\omega/c)^2}\right)\overline{F}_\mu(x,k_y,k_z,\omega)|_{x=0} = 0. \tag{24}$$

The first order differential equation (24) represents the absorbing boundary condition for the evanescent modes with the transverse wave number $\sqrt{k_y^2+k_z^2}$ incident on the boundary to the open half-space at $x = 0$.

For $k_y^2 + k_z^2 < (\omega/c)^2$, we introduce $\alpha_2 = \sqrt{k_y^2+k_z^2-(\omega/c)^2}$. Using [16]

$$\mathcal{L}^{-1}\left\{\frac{p}{p^2+\alpha_2^2}\right\} = \cos\alpha_2 x \tag{25}$$

and

$$\mathcal{L}^{-1}\left\{\frac{\alpha_2}{p^2+\alpha_2^2}\right\} = \sin\alpha_2 x \tag{26}$$

for $x \geq 0$ yields

$$\overline{F}_\mu(x,k_y,k_z,\omega) = \frac{e^{\jmath\alpha_2 x}}{2}\left(\overline{F}_\mu(x,k_y,k_z,\omega)|_{x=0} - \frac{\jmath}{\alpha_2}\frac{\partial\overline{F}_\mu(x,k_y,k_z,\omega)}{\partial x}\bigg|_{x=0}\right) + \frac{e^{-\jmath\alpha_2 x}}{2}\left(\overline{F}_\mu(x,k_y,k_z,\omega)|_{x=0} + \frac{\jmath}{\alpha_2}\frac{\partial\overline{F}_\mu(x,k_y,k_z,\omega)}{\partial x}\bigg|_{x=0}\right). \quad (27)$$

For $x \rightarrow \infty$, the function $\overline{F}_\mu(x,k_y,k_z,\omega)$ must represent an outgoing wave with respect to x. Therefore, we obtain

$$\overline{F}_\mu(x,k_y,k_z,\omega)|_{x=0} = \frac{\jmath}{\alpha_2}\frac{\partial\overline{F}_\mu(x,k_y,k_z,\omega)}{\partial x}\bigg|_{x=0} \quad (28)$$

and

$$\left(\frac{\partial}{\partial x} + \jmath\sqrt{(\omega/c)^2 - k_y^2 - k_z^2}\right)\overline{F}_\mu(x)|_{x=0} = 0 \quad (29)$$

respectively. The first order differential equation (29) represents the absorbing boundary condition for the propagating modes with the transverse wave number $\sqrt{k_y^2 + k_z^2}$ incident on the boundary to the open half-space at $x = 0$. The first order differential operator $(\partial/\partial x + \jmath\alpha_2)$ is equivalent to the first order differential boundary operator introduced by Engquist and Majda [17]. Approximating this first order differential boundary operator yields the most commonly used absorbing boundary conditions for FDTD [17]–[19] and TLM [20], [21]. Modelling the absorbing boundary condition at the boundary to the open half-space, the wave pulses incident on the boundary to the open half-space are convolved with the analytic TLM Green's functions. As the calculation of the analytic TLM Green's functions is based on (23) and (28), the absorbing boundary condition using the analytic TLM Green's functions corresponds to an absorbing boundary condition absorbing both evanescent and propagating modes.

Wave amplitudes are related to transverse electric and magnetic field components. For a general definition of the relationship between the wave amplitudes and the electric and magnetic field components, we introduce the vector of the incident wave amplitudes

$$\boldsymbol{a} = 1/2(-\boldsymbol{n}\times\boldsymbol{n}\times\boldsymbol{E} + Z_0\boldsymbol{n}\times\boldsymbol{H}) \quad (30)$$

and the vector of the scattered wave amplitudes

$$\boldsymbol{b} = -1/2(\boldsymbol{n}\times\boldsymbol{n}\times\boldsymbol{E} + Z_0\boldsymbol{n}\times\boldsymbol{H}) \quad (31)$$

for the boundary of an arbitrary spatial domain. The vector $\boldsymbol{n}$ is the outward directed unit vector normal to the boundary surface of the spatial domain. For three-dimensional TLM, Z_0 is the wave impedance of the free space. For example, sampling the vectors of the incident and scattered wave amplitudes in the boundary surfaces of a three-dimensional TLM cell yields the cell boundary mapping [6]. For the open half-space with $x \geq 0$, the vector $\boldsymbol{n}$ in cartesian components is given by $\boldsymbol{n} = [-1,0,0]^T$. With $\boldsymbol{a} = [a_x, a_1, a_3]^T$ and $\boldsymbol{b} = [b_x, b_1, b_3]^T$, (30) and (31) yield the continuous incident and scattered wave amplitudes for the open half-space with $x \geq 0$

$$\begin{aligned} a_1(y,z,t) &= 1/2(E_y(\vec{x},t) + Z_0H_z(\vec{x},t))|_{x=0},\\ b_1(y,z,t) &= 1/2(E_y(\vec{x},t) - Z_0H_z(\vec{x},t))|_{x=0},\\ a_3(y,z,t) &= 1/2(E_z(\vec{x},t) - Z_0H_y(\vec{x},t))|_{x=0},\\ b_3(y,z,t) &= 1/2(E_z(\vec{x},t) + Z_0H_y(\vec{x},t))|_{x=0},\\ a_x(y,z,t) &= 0,\\ b_x(y,z,t) &= 0. \end{aligned} \quad (32)$$

For the calculation of the analytic TLM Green's functions corresponding to the discrete TLM Green's functions G^{11} and G^{31}, we choose the localized electromagnetic excitation

$$\begin{aligned} a_1(y,z,t) &= f_{yz}(y,z)f_t(t),\\ a_3(y,z,t) &= 0. \end{aligned} \quad (33)$$

The function $f_{yz}(y,z)$ describes the spatial distribution of the localized electromagnetic excitation $a_1(y,z,t)$, the function $f_t(t)$ describes the time dependence of $a_1(y,z,t)$. In spectral domain, (33) yields

$$\begin{aligned} \overline{a}_1(k_y,k_z,\omega) &= \overline{f}_{yz}(k_y,k_z)\overline{f}_t(\omega),\\ \overline{a}_3(k_y,k_z,\omega) &= 0. \end{aligned} \quad (34)$$

Maxwell's equation may be written in spectral domain with respect to the coordinates ω, k_y and k_z as

$$\begin{aligned} k_y\overline{H}_z - k_z\overline{H}_y &= \frac{\omega}{cZ_0}\overline{E}_x,\\ \jmath k_z\overline{H}_x - \frac{\partial\overline{H}_z}{\partial x} &= \jmath\frac{\omega}{cZ_0}\overline{E}_y,\\ \frac{\partial\overline{H}_y}{\partial x} - \jmath k_y\overline{H}_x &= \jmath\frac{\omega}{cZ_0}\overline{E}_z,\\ k_y\overline{E}_z - k_z\overline{E}_y &= -\frac{\omega Z_0}{c}\overline{H}_x,\\ \jmath k_z\overline{E}_x - \frac{\partial\overline{E}_z}{\partial x} &= -\jmath\frac{\omega Z_0}{c}\overline{H}_y,\\ \frac{\partial\overline{E}_y}{\partial x} - \jmath k_y\overline{E}_x &= -\jmath\frac{\omega Z_0}{c}\overline{H}_z. \end{aligned} \quad (35)$$

We consider Maxwell's equations for $x = 0$ and eliminate the partial derivatives with respect to x by inserting the boundary conditions (23) and (28). Introducing the continuous incident and scattered wave amplitudes for the open half-space with $x \geq 0$ and inserting (34) yields

$$\begin{aligned} \overline{b}_1(0) &= \overline{f}_{yz}(k_y,k_z)\overline{f}_t(\omega)\overline{\mathcal{G}}_{11}(k_y,k_z,\omega),\\ \overline{b}_3(0) &= \overline{f}_{yz}(k_y,k_z)\overline{f}_t(\omega)\overline{\mathcal{G}}_{31}(k_y,k_z,\omega) \end{aligned} \quad (36)$$

where we have introduced the Green's functions in spectral domain, $\overline{\mathcal{G}}_{11}(k_y,k_z,\omega)$ and $\overline{\mathcal{G}}_{31}(k_y,k_z,\omega)$, given by

$$\begin{aligned} \overline{\mathcal{G}}_{11}(k_y,k_z,\omega) &= \frac{k_z^2 - k_y^2}{(k_z^2+k_y^2)^2}\left(\frac{2\omega^2}{c^2} - k_y^2 - k_z^2 + \jmath\frac{2\omega}{c}\alpha_1\right),\\ \overline{\mathcal{G}}_{31}(k_y,k_z,\omega) &= -\frac{2k_yk_z}{(k_z^2+k_y^2)^2}\left(\frac{2\omega^2}{c^2} - k_y^2 - k_z^2 + \jmath\frac{2\omega}{c}\alpha_1\right) \end{aligned} \quad (37)$$

for $k_y^2 + k_z^2 > (\omega/c)^2$ and

$$\overline{\mathcal{G}}_{11}(k_y, k_z, \omega) = \frac{k_z^2 - k_y^2}{(k_z^2 + k_y^2)^2}\left(\frac{2\omega^2}{c^2} - k_y^2 - k_z^2 - \frac{2\omega}{c}\alpha_2\right),$$
$$\overline{\mathcal{G}}_{31}(k_y, k_z, \omega) = -\frac{2k_y k_z}{(k_z^2 + k_y^2)^2}\left(\frac{2\omega^2}{c^2} - k_y^2 - k_z^2 - \frac{2\omega}{c}\alpha_2\right) \tag{38}$$

for $k_y^2 + k_z^2 < (\omega/c)^2$. As shown in the appendix, the Green's functions $\mathcal{G}_{11}(y, z, t)$ and $\mathcal{G}_{31}(y, z, t)$ may be calculated as

$$\mathcal{G}_{11}(r, \varphi, t) = -\delta\left(t - \frac{r}{c}\right)\frac{\cos(2\varphi)}{\pi r^2} \tag{39}$$

and

$$\mathcal{G}_{31}(r, \varphi, t) = -\delta\left(t - \frac{r}{c}\right)\frac{\sin(2\varphi)}{\pi r^2}, \tag{40}$$

where we have used

$$y = r\cos\varphi,$$
$$z = r\sin\varphi. \tag{41}$$

With these results (36) yields

$$b_1(y, z, t) = \mathcal{G}_{11}(y, z, t) * a_1(y, z, t)$$
$$= \frac{1}{\pi}\int_{-\infty}^{\infty}\int_{-\infty}^{\infty} f_{yz}(\eta - y, \xi - z)$$
$$f_t\left(t - \frac{1}{c}\sqrt{\eta^2 + \xi^2}\right)\frac{\xi^2 - \eta^2}{(\xi^2 + \eta^2)^2}\, d\eta\, d\xi \tag{42}$$

and

$$b_3(y, z, t) = \mathcal{G}_{31}(y, z, t) * a_3(y, z, t)$$
$$= -\frac{1}{\pi}\int_{-\infty}^{\infty}\int_{-\infty}^{\infty} f_{yz}(\eta - y, \xi - z)$$
$$f_t\left(t - \frac{1}{c}\sqrt{\eta^2 + \xi^2}\right)\frac{2\xi\eta}{(\xi^2 + \eta^2)^2}\, d\eta\, d\xi. \tag{43}$$

Choosing a delta distribution as the spatial distribution of $a_1(y, z, t)$, the function $f_{yz}(y, z)$ is given by

$$f_{yz}(y, z) = \delta(y)\delta(z)(\Delta l)^2 \tag{44}$$

and therefore

$$\overline{f}_{yz}(k_y, k_z) = (\Delta l)^2. \tag{45}$$

We denote the functions $b_1(y, z, t)$ and $b_3(y, z, t)$ due to a delta distribution as the spatial distribution of $a_1(y, z, t)$ by $b_1^\delta(y, z, t)$ and $b_3^\delta(y, z, t)$. Equations (42) and (43) yield

$$b_1^\delta(r, \varphi, t) = -f_t\left(t - \frac{r}{c}\right)\cos(2\varphi)\frac{(\Delta l)^2}{\pi r^2} \tag{46}$$

and

$$b_3^\delta(r, \varphi, t) = -f_t\left(t - \frac{r}{c}\right)\sin(2\varphi)\frac{(\Delta l)^2}{\pi r^2}. \tag{47}$$

For a two-dimensional pulse function as the spatial distribution of $a_1(y, z, t)$

$$f_{yz}(y, z) = h(y)h(z), \tag{48}$$

with

$$h(x) = \begin{cases} 1 & \text{for } |x| < 1/2 \\ 1/2 & \text{for } |x| = 1/2 \\ 0 & \text{for } |x| > 1/2, \end{cases} \tag{49}$$

we obtain

$$b_1^P(y, z, t) = \frac{1}{\pi}\int_{y-(\Delta l/2)}^{y+(\Delta l/2)}\int_{z-(\Delta l/2)}^{z+(\Delta l/2)} f_t$$
$$\cdot\left(t - \frac{1}{c}\sqrt{\eta^2 + \xi^2}\right)\frac{\xi^2 - \eta^2}{(\xi^2 + \eta^2)^2}\, d\eta\, d\xi \tag{50}$$

and

$$b_3^P(y, z, t) = -\frac{1}{\pi}\int_{y-(\Delta l/2)}^{y+(\Delta l/2)}\int_{z-(\Delta l/2)}^{z+(\Delta l/2)} f_t$$
$$\cdot\left(t - \frac{1}{c}\sqrt{\eta^2 + \xi^2}\right)\frac{2\xi\eta}{(\xi^2 + \eta^2)^2}\, d\eta\, d\xi. \tag{51}$$

The two-dimensional triangle function

$$f_{yz}(y, z) = g(y)g(z) \tag{52}$$

with

$$g(x) = \begin{cases} 1 - |x| & \text{for } |x| < 1 \\ 0 & \text{for } |x| \geq 1 \end{cases} \tag{53}$$

represents the spatial distribution of the localized excitation corresponding to the expansion functions used in the field theoretic derivation of the condensed symmetric node [6], [7]. In this case, we have

$$b_1^T(y, z, t) = \frac{1}{\pi}\int_{y-\Delta l}^{y+\Delta l}\int_{z-\Delta l}^{z+\Delta l} g(\eta - y)g(\xi - z)f_t$$
$$\cdot\left(t - \frac{1}{c}\sqrt{\eta^2 + \xi^2}\right)\frac{\xi^2 - \eta^2}{(\xi^2 + \eta^2)^2}\, d\eta\, d\xi \tag{54}$$

and

$$b_3^T(y, z, t) = -\frac{1}{\pi}\int_{y-\Delta l}^{y+\Delta l}\int_{z-\Delta l}^{z+\Delta l} g(\eta - y)g(\xi - z)f_t$$
$$\cdot\left(t - \frac{1}{c}\sqrt{\eta^2 + \xi^2}\right)\frac{2\xi\eta}{(\xi^2 + \eta^2)^2}\, d\eta\, d\xi. \tag{55}$$

The analytic TLM Green's functions are defined as the discretized response to a localized electromagnetic excitation. The continuous response to the localized electromagnetic excitation $a_1(y, z, t)$ at the boundary of the open half-space is described by the functions $b_1(y, z, t)$ and $b_3(y, z, t)$. Thus the analytic TLM Green's functions are obtained by discretizing the functions $b_1(y, z, t)$ and $b_3(y, z, t)$. Using delta functions, we sample the functions $b_1(y, z, t)$ and $b_3(y, z, t)$ at the discrete space points $y = m\Delta l$ and $z = n\Delta l$ and at the discrete time points $t = k\Delta t$. The analytic TLM Green's functions are the functions $G_{11}(m, n, k)$ and $G_{31}(m, n, k)$ given by

$$G_{11}(m, n, k) = \int_{-\infty}^{+\infty}\int_{-\infty}^{+\infty}\int_{-\infty}^{+\infty} b_1(y, z, t)\delta(y - m\Delta l)$$
$$\cdot\,\delta(z - n\Delta l)\delta(t - k\Delta t)\, dy\, dz\, dt \tag{56}$$

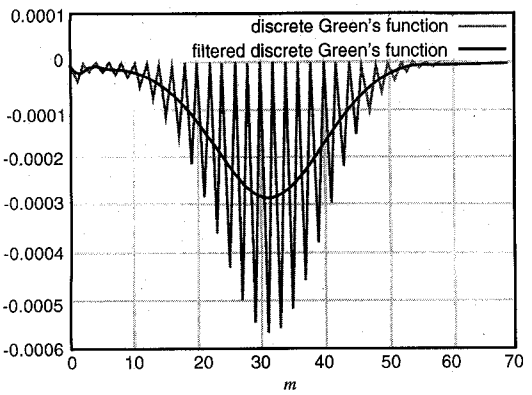

Fig. 2. The function ${}_{71}G^{11g}_{m,0}$ and the filtered function ${}_{71}\tilde{G}^{11g}_{m,0}$.

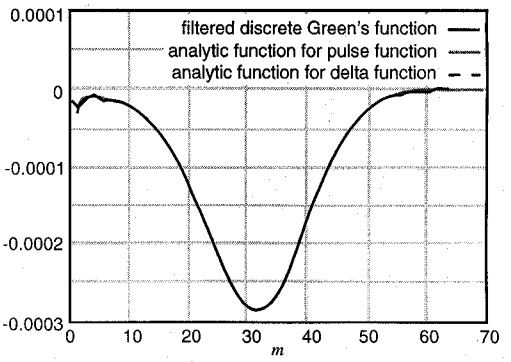

Fig. 3. The analytic TLM Green's functions and ${}_{71}\tilde{G}^{11g}_{m,0}$.

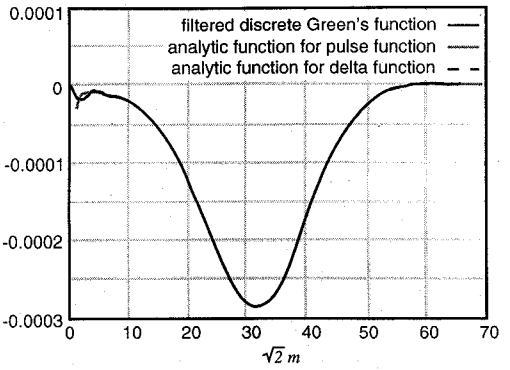

Fig. 4. The analytic TLM Green's functions and ${}_{71}\tilde{G}^{31g}_{m,m}$.

and

$$G_{31}(m,n,k) = \int_{-\infty}^{+\infty}\int_{-\infty}^{+\infty}\int_{-\infty}^{+\infty} b_3(y,z,t)\delta(y-m\Delta l) \cdot \delta(z-n\Delta l)\delta(t-k\Delta t)\,dy\,dz\,dt. \quad (57)$$

After having shown the identity of the discrete and the analytic TLM Green's functions for low frequencies and small wave numbers, we will replace the discrete TLM Green's function in (5) by the analytic TLM Green's function. This enables us to model the absorbing boundary condition at the boundary of the open half-space using analytic TLM Green's function.

IV. Comparison of the Discrete and the Analytic TLM Green's Functions

Since TLM gives only a correct description of the field evolution for signals with a frequency spectrum bounded sufficiently below the TLM cutoff frequency [2], [3], we assume a Gaussian excitation of the open half-space with respect to time. For the numerical calculation of the discrete TLM Green's functions ${}_kG^{11g}_{m,n}$ and ${}_kG^{13g}_{m,n}$, we choose the excitation

$$f_t(k\Delta t) = e^{-(k\Delta t)^2/2\sigma^2)} \quad (58)$$

with the pulse width $\sigma = 16\Delta t$ in port 1 of the boundary node $(m,n) = (0,0)$. The index g indicates that we have used a Gaussian excitation with respect to the discrete time coordinate k. In Fig. 2, the function ${}_{71}G^{11g}_{m,0}$ is depicted for $m \geq 0$. The discrete TLM Green's function consists of physical modes with small wave numbers as well as of spurious modes with large wave numbers and $k_y = \pi/\Delta l$, respectively. To avoid the spurious modes, we filter the discrete TLM Green's function with a low-pass filter in spectral domain and obtain the filtered discrete TLM Green's functions ${}_k\tilde{G}^{11g}_{m,n}$ and ${}_k\tilde{G}^{31g}_{m,n}$, respectively. The function ${}_{71}\tilde{G}^{11g}_{m,0}$ is also shown in Fig. 2.

Figs. 3 and 4 show that the analytic TLM Green's functions and the discrete TLM Green's functions are identical for low frequencies and small wave numbers. The functions ${}_{71}\tilde{G}^{11g}_{m,0}$ and ${}_{71}\tilde{G}^{31g}_{m,m}$ are compared with the analytic TLM Green's functions for two different localized electromagnetic excitations at the boundary to the open half-space. The response to the localized excitation is given by a spherical wave reflected from the boundary. For small wave numbers and $[k_y,k_z]^T \ll [\pi/\Delta l, \pi/\Delta l]^T$, respectively, the analytic TLM Green's functions for a delta function, $G^\delta(m,n,k)$, a two-dimensional pulse function, $G^P(m,n,k)$, and a two-dimensional triangle function, $G^T(m,n,k)$, as the spatial distribution of the localized electromagnetic excitation are identical. Thus, for small wave numbers and for small frequencies $f \ll 1/(2\Delta t)$, due to the linearity of the convolution, the application of the functions $G^\delta(m,n,k), G^P(m,n,k)$ or $G^T(m,n,k)$ in modelling the absorbing boundary condition at the boundary of the open half-space will give the same results.

As a consequence of the singularity of the analytic TLM Green's functions at $(m,n) = (0,0)$, there are deviations of ${}_{71}\tilde{G}^{11g}_{m,0}$ and ${}_{71}\tilde{G}^{31g}_{m,m}$ from the analytic TLM Green's functions for $m \approx 0$ due to errors in the filtering of the discrete Green's functions. To determine the values of the analytic TLM Green's functions at $m = 0$ and $n = 0$, we calculate $G^P_{11}(0,0,k)$ and $G^P_{31}(0,0,k)$ for an arbitrary excitation with respect to time. Equation (51) yields

$$G^P_{31}(0,0,k) = -\frac{1}{\pi}\int_{-(\Delta l/2)}^{(\Delta l/2)}\int_{-(\Delta l/2)}^{(\Delta l/2)} f_t \cdot \left(k\Delta t - \frac{1}{c}\sqrt{\eta^2+\xi^2}\right) \cdot \frac{2\xi\eta}{(\xi^2+\eta^2)^2}\,d\eta\,d\xi = 0 \quad (59)$$

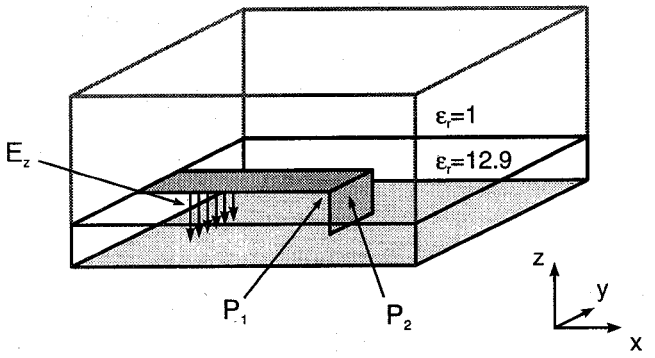

Fig. 5. A short-circuited microstrip line.

because the integrand is an odd function in η and ξ. From (50), we calculate

$$\begin{aligned} G_{11}^{P}(0,0,k) &= \frac{4}{\pi}\int_{\eta=0}^{\Delta l/2}\int_{\xi=0}^{\Delta l/2} f_t\left(k\Delta t - \frac{1}{c}\sqrt{\eta^2+\xi^2}\right) \\ &\quad \cdot \frac{\xi^2-\eta^2}{(\xi^2+\eta^2)^2}\, d\eta\, d\xi \\ &= -\frac{4}{\pi}\int_{\varphi=0}^{\pi/4}\int_{r=0}^{\Delta l/2\cos\varphi} f_t\left(k\Delta t - \frac{r}{c}\right) \\ &\quad \cdot \frac{\cos(2\varphi)}{r}\, dr\, d\varphi - \frac{4}{\pi}\int_{\varphi=\pi/4}^{\pi/2}\int_{r=0}^{\Delta l/2\sin\varphi) } f_t \\ &\quad \cdot \left(k\Delta t - \frac{r}{c}\right)\frac{\cos(2\varphi)}{r}\, dr\, d\varphi \\ &= I_1 + I_2. \end{aligned} \tag{60}$$

Substituting $\varphi' = \pi/2 - \varphi$ in the integral I_2 yields $I_2 = -I_1$ and

$$G_{11}^{P}(0,0,k) = 0 \tag{61}$$

respectively. In the same way, we may calculate

$$G_{11}^{T}(0,0,k) = 0 \tag{62}$$

and

$$G_{31}^{T}(0,0,k) = 0. \tag{63}$$

As the two-dimensional pulse function is converging at the two-dimensional delta distribution for small pulse widths and large pulse amplitudes, we also apply

$$G_{11}^{\delta}(0,0,k) = 0 \tag{64}$$

and

$$G_{31}^{\delta}(0,0,k) = 0 \tag{65}$$

when modelling the absorbing boundary condition at the boundary to the open half-space using the functions $G^{\delta}(m,n,k)$.

V. Absorbing Boundary Conditions Using the Analytic TLM Green's Functions

As an example, we analyze the lossless microstrip line depicted in Fig. 5. The microstrip line is short circuited and thus, it represents a simple model of a via hole. The width of the microstrip line is 160 μm. The non-magnetic substrate with the dielectric constant $\varepsilon_r = 12.9$ has the thickness of 140 μm. Above the microstrip line, there is the open half-space with $\varepsilon_r = 1$. We excite the z-component of the electric field with a constant amplitude with respect to the y- and z-coordinate and with a gaussian time dependence according to (58) with $\sigma = 40\Delta t$. We choose the length interval $\Delta l = 20\,\mu$m and the time interval $\Delta t = 0.0333$ ps, respectively.

The absorbing boundary condition at the boundary of the open half-space is modelled by convolving the wave pulses incident on the boundary to the open half-space with the discrete TLM Green's functions and with the analytic TLM Green's functions, respectively. In a computer simulation, the convolution has to be truncated with respect to space and time. Using the John's matrix representation [9], the discrete TLM Green's functions may be represented by matrices. We approximate the discrete TLM Green's functions by $K+1$ matrices of the size $(M+1)\times(N+1)$. Applying the symmetry relations of the discrete TLM Green's functions, (5) yields

$$\begin{aligned} {}_k[b_1]_{0,m,n} &= \sum_{m'=m-M/2}^{m+M/2}\sum_{n'=n-N/2}^{n+N/2}\sum_{k'=k-K}^{k} \\ &\quad \cdot {}_{k-k'}G^{11}_{m-m',n-n'\ k'}[a_1]_{0,m',n'} \\ &\quad + \sum_{m'=m-M/2}^{m+M/2}\sum_{n'=n-N/2}^{n+N/2}\sum_{k'=k-K}^{k} \\ &\quad \cdot {}_{k-k'}G^{31}_{m-m',n-n'\ k'}[a_3]_{0,m',n'}, \\ {}_k[b_3]_{0,m,n} &= \sum_{m'=m-M/2}^{m+M/2}\sum_{n'=n-N/2}^{n+N/2}\sum_{k'=k-K}^{k} \\ &\quad \cdot {}_{k-k'}G^{31}_{m-m',n-n'\ k'}[a_1]_{0,m',n'} \\ &\quad - \sum_{m'=m-M/2}^{m+M/2}\sum_{n'=n-N/2}^{n+N/2}\sum_{k'=k-K}^{k} \\ &\quad \cdot {}_{k-k'}G^{11}_{m-m',n-n'\ k'}[a_3]_{0,m',n'}. \end{aligned} \tag{66}$$

Equation (66) has been applied in the simulation of the short-circuited microstrip line using discrete TLM Green's functions. Due to the convolution with respect to m,n and k and to three dimensions, respectively, the computation time is enormous. Furthermore, as the absorbing boundary condition has been placed directly above the microstrip line, instability has occurred due to spurious modes with large wave vectors and $[k_x,k_y,k_z] \approx [\pi/\Delta l, \pi/\Delta l, \pi/\Delta l]$, respectively, near the discontinuity [22].

The analytic TLM Green's functions represent the discretized response to a localized excitation. Choosing

$$f_t(k\Delta t) = h(k\Delta t) \tag{67}$$

the response to the localized excitation is given by a spherical wave which is bounded close around a sphere with the radius

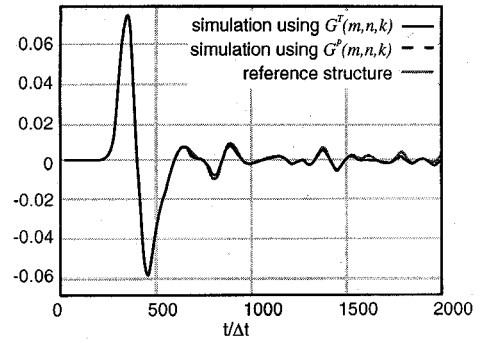

Fig. 6. Pulse and triangle functions as localized excitation at the boundary; E_z at the observation point P_1.

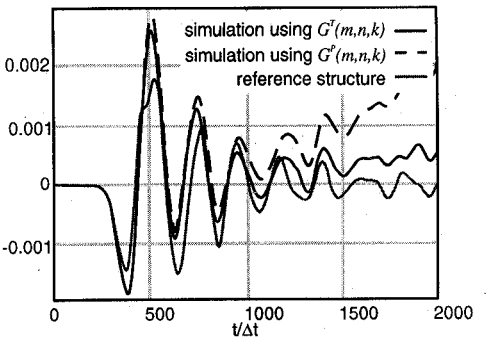

Fig. 7. Pulse and triangle functions as localized excitation at the boundary; E_z at the observation point P_2.

$r = ct$, where c is the free space velocity of light. Thus the convolution may be restricted to a set of pulses in a neighbourhood of this sphere and the convolution with respect to k' may be eliminated. Replacing the discrete TLM Green's functions by $G^\delta(m,n,k)$, we obtain from (66)

$$
\begin{aligned}
{}_k[b_1]_{0,m,n} = & \sum_{m'=m-M/2}^{m+M/2} \sum_{n'=n-N/2}^{n+N/2} \\
& \cdot \frac{(n-n')^2-(m-m')^2}{\pi((n-n')^2+(m-m')^2)^2}\, {}_{k-k_\delta}[a_1]_{0,m',n'} \\
& + \sum_{m'=m-M/2}^{m+M/2} \sum_{n'=n-N/2}^{n+N/2} \\
& \cdot \frac{2(n-n')(m-m')}{\pi((n-n')^2+(m-m')^2)^2}\, {}_{k-k_\delta}[a_3]_{0,m',n'}, \\
{}_k[b_3]_{0,m,n} = & \sum_{m'=m-M/2}^{m+M/2} \sum_{n'=n-N/2}^{n+N/2} \\
& \cdot \frac{2(n-n')(m-m')}{\pi((n-n')^2+(m-m')^2)^2}\, {}_{k-k_\delta}[a_1]_{0,m',n'} \\
& - \sum_{m'=m-M/2}^{m+M/2} \sum_{n'=n-N/2}^{n+N/2} \\
& \cdot \frac{(n-n')^2-(m-m')^2}{\pi((n-n')^2+(m-m')^2)^2}\, {}_{k-k_\delta}[a_3]_{0,m',n'}
\end{aligned}
\tag{68}
$$

where k_δ represents a positive integer determined by

$$
\begin{aligned}
-1/2+2\sqrt{(m-m')^2+(n-n')^2} < k_\delta \\
< 1/2+2\sqrt{(m-m')^2+(n-n')^2}.
\end{aligned}
\tag{69}
$$

The convolution according to (68) has been tested in the simulation of the short-circuited microstrip line. Due to the delta distribution as spatial distribution of the localized excitation, the analytic TLM Green's functions incorporate parts with large wave numbers leading to a strong instability of the convolution due to the amplification of the spurious modes at the boundary [22]. The functions $G^P(m,n,k)$ and $G^T(m,n,k)$ incorporate less parts with large wave numbers which results in a much more stable absorbing boundary condition. Assuming a time dependence according to (67), the convolution with $G^P(m,n,k)$ is given by

$$
\begin{aligned}
{}_k[b_1]_{0,m,n} = & \sum_{m'=m-M/2}^{m+M/2} \sum_{n'=n-N/2}^{n+N/2} \sum_{k_P} \\
& \cdot G^P_{11}(m-m',n-n',k_P)\, {}_{k-k_P}[a_1]_{0,m',n'} \\
& + \sum_{m'=m-M/2}^{m+M/2} \sum_{n'=n-N/2}^{n+N/2} \sum_{k_P} \\
& \cdot G^P_{31}(m-m',n-n',k_P)\, {}_{k-k_P}[a_3]_{0,m',n'}, \\
{}_k[b_3]_{0,m,n} = & \sum_{m'=m-M/2}^{m+M/2} \sum_{n'=n-N/2}^{n+N/2} \sum_{k_P} \\
& \cdot G^P_{31}(m-m',n-n',k_P)\, {}_{k-k_P}[a_1]_{0,m',n'} \\
& - \sum_{m'=m-M/2}^{m+M/2} \sum_{n'=n-N/2}^{n+N/2} \sum_{k_P} \\
& \cdot G^P_{11}(m-m',n-n',k_P)\, {}_{k-k_P}[a_3]_{0,m',n'},
\end{aligned}
\tag{70}
$$

where k_P represents a positive integer with

$$
\begin{aligned}
-1/2-\sqrt{2}+2\sqrt{(m-m')^2+(n-n')^2} < k_P < 1/2 \\
+\sqrt{2}+2\sqrt{(m-m')^2+(n-n')^2}.
\end{aligned}
\tag{71}
$$

The positive integer k_P may have up to four different values, so that the summation of k_P in (70) consists of up to four terms. In case of assuming the time dependence

$$
f_t(k\Delta t) = g(k\Delta t) \tag{72}
$$

and applying the functions $G^T(m,n,k)$, we have to replace k_P by the positive integer k_T determined by

$$
\begin{aligned}
-1-2\sqrt{2}+2\sqrt{(m-m')^2+(n-n')^2} < k_T < 1 \\
+2\sqrt{2}+2\sqrt{(m-m')^2+(n-n')^2}
\end{aligned}
\tag{73}
$$

so that the summation of k_T in (70) consists of up to eight terms.

Figs. 6 and 7 depict the TLM results of a simulation of the short circuited microstrip line using the functions $G^P(m,n,k)$ and $G^T(m,n,k)$ with $M = N = 60$. For the reference

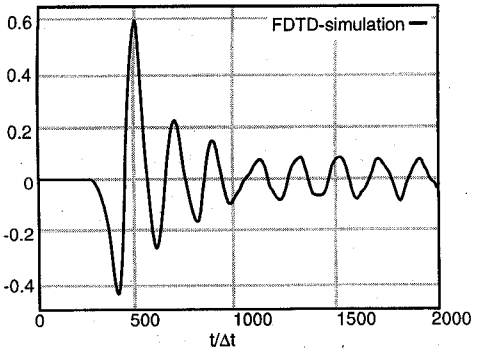

Fig. 8. FDTD-simulation of the reference structure; E_z at P_2.

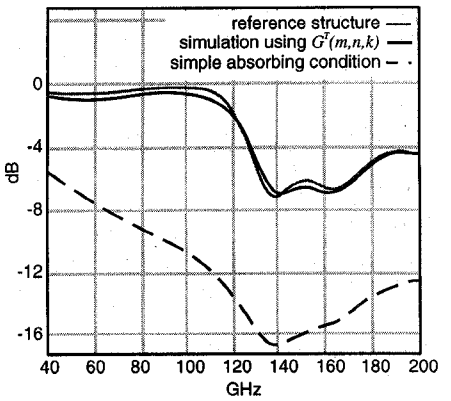

Fig. 9. The magnitude of the reflection coefficient; TLM-simulations.

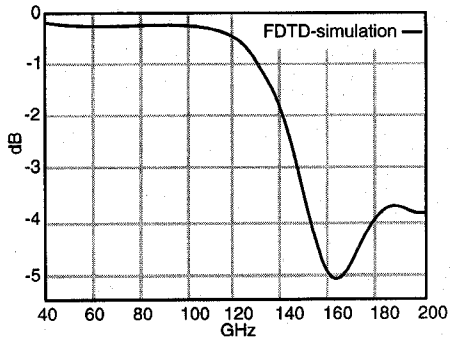

Fig. 10. The magnitude of the reflection coefficient; FDTD-simulation.

structure, the open half-space above the microstrip line has been approximated by a large TLM mesh. The observation point P_1 is situated directly under the microstrip line, the observation point P_2 is located near the discontinuity. As the absorbing boundary condition is placed directly above the microstrip line, instability at P_2 is observed due to spurious modes excited at the discontinuity [22]. As the spectrum of the two-dimensional triangle function contains less parts with large wave numbers than the spectrum of the two-dimensional pulse function, the application of $G^T(m,n,k)$ leads to a higher stability of the absorbing boundary condition than the application of $G^P(m,n,k)$. The instability of the absorbing boundary condition using the functions $G^P(m,n,k)$ and $G^T(m,n,k)$ is about the same as the instability of the absorbing boundary condition using the discrete TLM Green's functions.

Fig. 8 shows the electric field obtained by a simulation of the reference structure at P_2 using the FDTD-method. Due to a different implementation of the source, the values of the electric field amplitudes differ from the values of the electric field amplitudes calculated by the TLM-method. With respect to the first positive maximum at $t = 500\ \Delta t$, the FDTD result agrees well with the results obtained by the TLM simulations using the analytic TLM Green's functions, but differs from the result obtained by the TLM simulation of the reference structure. In the TLM mesh, at the discontinuity, spurious modes are superimposed on the physical modes. In the FDTD mesh, these kind of spurious modes do not occur [13]. Thus the application of the analytic TLM Green's functions leads to results without spurious modes near the discontinuity.

Fig. 9 depicts the magnitude of the reflection coefficient for the short circuited microstrip line calculated by the TLM method. The influence of the open half-space has been simulated by a large TLM mesh (reference structure), by an absorbing boundary condition using the functions $G^T(m,n,k)$ and by a simple absorbing boundary condition. For the simple absorbing boundary condition, each port intersecting the boundary to the open half-space has been terminated by a reflection coefficient of zero. To prevent instabilities, for the simulation involving $G^T(m,n,k)$, a TLM mesh of $10\Delta l$ with $\varepsilon_r = 1$ has been inserted between the microstrip line and the boundary to the open half-space [22]. Beside the resonance at 140 GHz, the results obtained by the simulation of the reference structure and by the simulation using $G^T(m,n,k)$ agree well with the FDTD results shown in Fig. 10. By the observations from previous results, it is concluded that the resonance at 140 GHz is due to spurious modes near the discontinuity.

VI. Conclusion

The relationship between the discrete TLM Green's functions and analytic TLM Green's functions has been demonstrated. The TLM method with condensed symmetric node gives only a correct description of the field evolution for signals with a frequency below the TLM cutoff frequency and with a wave vector well below $[\pi/\Delta l, \pi/\Delta l, \pi/\Delta l]^T$. For this frequency and wave vector range, the analytic TLM Green's functions and the discrete TLM Green's functions are identical. Due to the definition of the discrete TLM Green's functions as the impulse response to a single wave pulse excitation, the complete frequency spectrum is excited when calculating the discrete TLM Green's functions. Therefore, in comparison with the analytic TLM Green's functions, the discrete TLM Green's functions contain additional spurious modes. Due to these spurious modes, the algebraic calculation of the discrete TLM Green's functions [14] is more complicated then the calculation of the analytic TLM Green's functions.

The calculation of the analytic TLM Green's functions is based on the first order differential boundary operator introduced by Engquist and Majda [17]. In contrast to the absorbing boundary conditions based on the approximation of this differential operator [17]–[21], the absorbing boundary condition considered in this paper incorporates the exact differential operator describing the absorption of both evanescent and propagating modes. Thus, the analytic TLM Green's functions allow an exact formulation of absorbing boundary conditions in TLM.

The absorbing boundary condition at the boundary of the open half-space is modelled by convolving the wave pulses incident on the boundary with the discrete TLM Green's functions and the analytic TLM Green's functions, respectively. For the analytic TLM Green's functions, the convolution may be reduced by one dimension to a convolution with respect to two-dimensional space only. Hence, the computational effort for an absorbing boundary condition using discrete TLM Green's functions can be reduced considerably when using the analytic TLM Green's functions. The analytic TLM Green's functions for three different localized electromagnetic excitations have been applied in modelling the absorbing boundary condition by analyzing a short circuited microstrip line. The parts with large wave numbers in the spectrum of the localized electromagnetic excitation affect the stability of the absorbing boundary condition. The smaller the parts with large wave numbers, the more stability can be achieved.

The application of the analytic TLM Green's functions leads to results without spurious modes near the discontinuity provided the boundary of the open half-space is placed near the discontinuity. However, placing the boundary of the open half-space near the discontinuity leads to a higher instability of the absorbing boundary condition due to the spurious modes excited at the discontinuity [22]. Reducing the parts with large wave numbers in the spectrum of the localized electromagnetic excitation, the instabilities may only be reduced but not removed. These instabilities due to spurious modes represent a clear drawback for the TLM method with condensed symmetric node. Therefore, future work is concentrated on the use of the distributed [2], [3] and asymmetric condensed TLM node [2], [3], [23]. In a TLM mesh with these nodes, spurious modes with large wave numbers do not contribute for small frequencies and thus, it is expected that the absorbing boundary conditions exhibit a higher stability.

APPENDIX
THE CALCULATION OF THE GREEN'S FUNCTIONS

Using (12) we obtain

$$\begin{aligned}\mathcal{G}_{11}(y,z,\omega) = &\frac{1}{4\pi^2}\int_{-\infty}^{\infty}\int_{-\infty}^{\infty}\frac{k_z^2-k_y^2}{(k_z^2+k_y^2)^2}\\ &\cdot\left(\frac{2\omega^2}{c^2}-k_y^2-k_z^2-\frac{2\omega}{c}\alpha_2\right)\\ &\cdot e^{\jmath(k_y y+k_z z)}\,dk_y\,dk_z\\ &= I_{11}+I_{12}+I_{13}\end{aligned} \tag{74}$$

for the Green's function $\mathcal{G}_{11}(y,z,\omega)$ in frequency domain. The integrals I_{11}, I_{12} and I_{13} are given by

$$\begin{aligned}I_{11} = &\frac{\omega^2}{2c^2\pi^2}\int_{-\infty}^{\infty}\int_{-\infty}^{\infty}\frac{k_z^2-k_y^2}{(k_z^2+k_y^2)^2}\\ &\cdot e^{\jmath(k_y y+k_z z)}\,dk_y\,dk_z,\\ I_{12} = &-\frac{1}{4\pi^2}\int_{-\infty}^{\infty}\int_{-\infty}^{\infty}\frac{k_z^2-k_y^2}{(k_z^2+k_y^2)}\\ &\cdot e^{\jmath(k_y y+k_z z)}\,dk_y\,dk_z,\end{aligned} \tag{75}$$

and

$$\begin{aligned}I_{13} = &-\frac{\omega}{2c\pi^2}\int_{k_z^2+k_y^2<(\omega^2/c^2)}\\ &\cdot\frac{k_z^2-k_y^2}{(k_z^2+k_y^2)^2}\,\alpha_2 e^{\jmath(k_y y+k_z z)}\,dk_y\,dk_z\\ &+\jmath\frac{\omega}{2c\pi^2}\int_{k_z^2+k_y^2>(\omega^2/c^2)}\\ &\cdot\frac{k_z^2-k_y^2}{(k_z^2+k_y^2)^2}\,\alpha_1 e^{\jmath(k_y y+k_z z)}\,dk_y\,dk_z.\end{aligned} \tag{76}$$

For the calculation of I_{11}, we substitute

$$\begin{aligned}k_y &= k\,\cos k_\varphi,\\ k_z &= k\sin k_\varphi\end{aligned} \tag{77}$$

and use (41). With

$$\cos^2 x - \sin^2 x = \cos(2x) \tag{78}$$

we obtain

$$\begin{aligned}I_{11} = &-\frac{\omega^2}{2c^2\pi^2}\int_{k=0}^{\infty}\int_{k_\varphi=0}^{2\pi}\frac{\cos(2k_\varphi)}{k}\\ &\cdot e^{\jmath kr\cos(k_\varphi-\varphi)}\,dk\,dk_\varphi.\end{aligned} \tag{79}$$

Substituting $k_\varphi - \varphi = x$ and applying

$$\cos(2x+2\varphi) = \cos(2x)\cos(2\varphi) - \sin(2x)\sin(2\varphi) \tag{80}$$

yields

$$I_{11} = -\cos(2\varphi)\frac{\omega^2}{c^2\pi^2}\int_{k=0}^{\infty}\int_{x=0}^{\pi}\frac{\cos(2x)}{k}\,e^{\jmath kr\cos x}\,dk\,dx. \tag{81}$$

With [24]

$$\int_{x=0}^{\pi}\cos(2x)e^{\jmath\beta\cos x}\,dx = -\pi J_2(\beta) \tag{82}$$

and [25]

$$\int_{x=0}^{\infty}\frac{J_2(ax)}{x}\,dx = \frac{1}{2} \tag{83}$$

we obtain

$$I_{11} = \cos(2\varphi)\frac{\omega^2}{2c^2\pi}. \tag{84}$$

The function $J_2(x)$ represents the Bessel function of the first kind and of second order. The second integral I_{12} may be written as

$$I_{12} = -\frac{1}{\pi^2}\int_0^{\infty}\int_0^{\infty}\frac{k_z^2-k_y^2}{(k_z^2+k_y^2)}\cos(k_y y)\cos(k_z z)\,dk_y\,dk_z. \tag{85}$$

Using [26]

$$\int_0^{\infty}\frac{\cos(ax)}{(\beta^2+x^2)}\,dx = \frac{\pi}{2\beta}e^{-a\beta} \tag{86}$$

for $a \geq 0$ and $\Re\{\beta\} > 0$ as well as [27]

$$\int_0^\infty x e^{-ax} \cos(\beta x)\, dx = \frac{a^2 - \beta^2}{(a^2+\beta^2)^2} \tag{87}$$

we calculate

$$I_{12} = \frac{1}{\pi} \frac{z^2 - y^2}{(z^2+y^2)^2} \tag{88}$$

and

$$I_{12} = -\frac{\cos(2\varphi)}{\pi r^2} \tag{89}$$

respectively. The third integral I_{13} may be calculated in a way analogous with the calculation of I_{11}. We substitute (77), use (41) and solve the integral with respect to k_φ with the help of (78), (80) and (82). We obtain

$$I_{13} = -\cos(2\varphi)\frac{\omega}{c\pi} \int_{k=0}^{\omega/c} \frac{J_2(kr)}{k} \sqrt{\frac{\omega^2}{c^2} - k^2}\, dk + \jmath \cos(2\varphi)\frac{\omega}{c\pi} \int_{k=\omega/c}^{\infty} \frac{J_2(kr)}{k} \sqrt{k^2 - \frac{\omega^2}{c^2}}\, dk. \tag{90}$$

Substituting $k = x\omega/c$ yields

$$I_{13} = -\cos(2\varphi)\frac{\omega^2}{c^2\pi} \int_{x=0}^{1} \frac{J_2\left(x\frac{r\omega}{c}\right)}{x} \sqrt{1-x^2}\, dx + \jmath \cos(2\varphi)\frac{\omega^2}{c^2\pi} \int_{x=1}^{\infty} \frac{J_2\left(x\frac{r\omega}{c}\right)}{x} \sqrt{x^2-1}\, dx. \tag{91}$$

Applying the integrals [28]

$$\int_{x=0}^{1} \frac{J_2(ax)}{x} \sqrt{1-x^2}\, dx = \frac{1}{2} - \frac{1}{a^2} + \frac{\cos a}{a^2} \tag{92}$$

and [29]

$$\int_{x=1}^{\infty} \frac{J_2(ax)}{x} \sqrt{x^2-1}\, dx = \frac{\sin a}{a^2} \tag{93}$$

yields

$$I_{13} = \frac{\cos(2\varphi)}{\pi}\left(-\frac{\omega^2}{2c^2} + \frac{1}{r^2} - \frac{1}{r^2} e^{-\jmath r(\omega/c)}\right). \tag{94}$$

For the Green's function $\mathcal{G}_{11}(r, \varphi, \omega)$ in frequency domain, we obtain

$$\mathcal{G}_{11}(r, \varphi, \omega) = -\frac{\cos(2\varphi)}{\pi r^2} e^{-\jmath r\omega/c} \tag{95}$$

and with

$$\mathcal{F}^{-1}\{e^{-\jmath\omega t_0}\} = \delta(t - t_0) \tag{96}$$

the Green's function $\mathcal{G}_{11}(r, \varphi, t)$ in time domain given by (39).

The calculation of the Green's function $\mathcal{G}_{31}(y, z, \omega)$ is done in a similar way. We obtain

$$\mathcal{G}_{31}(y, z, \omega) = I_{31} + I_{32} + I_{33}, \tag{97}$$

where

$$I_{31} = \sin(2\varphi)\frac{\omega^2}{2c^2\pi}, \qquad I_{32} = -\frac{\sin(2\varphi)}{\pi r^2}, \tag{98}$$

and

$$I_{33} = \frac{\sin(2\varphi)}{\pi}\left(-\frac{\omega^2}{2c^2} + \frac{1}{r^2} - \frac{1}{r^2} e^{-\jmath r(\omega/c)}\right). \tag{99}$$

Applying (96) yields the function $\mathcal{G}_{31}(r, \varphi, t)$ in time domain given by (40). The calculation of I_{31} and I_{33} has been done analogously with the calculation of I_{11} and I_{13}. Additionally, we have used the relations

$$2 \sin x \cos x = \sin(2x) \tag{100}$$

and

$$\sin(2x + 2\varphi) = \sin(2x)\cos(2\varphi) + \cos(2x)\sin(2\varphi). \tag{101}$$

For the calculation of I_{32}, we have applied [30]

$$\int_0^\infty \frac{x \sin(ax)}{(\beta^2 + x^2)}\, dx = \frac{\pi}{2} e^{-a\beta} \tag{102}$$

and [31]

$$\int_0^\infty x e^{-ax} \sin(\beta x)\, dx = \frac{2a\beta}{(a^2+\beta^2)^2}. \tag{103}$$

ACKNOWLEDGMENT

The authors would like to thank Dr. Luca Roselli from the University of Perugia, Italy, for calculating the FDTD reference data.

REFERENCES

[1] G. Kron, "Equivalent circuit of the field equations of Maxwell I," *Proc. IRE,* vol. 32, pp. 289–299, May 1944.

[2] W. J. R. Hoefer, "The transmission line matrix method-theory and applications," *IEEE Trans. Microwave Theory Tech.,* vol. MTT-33, no. 10, pp. 882–893, Oct. 1985.

[3] ——, "The transmission line matrix (TLM) method," in *Numerical Techniques for Microwave and Millimeter Wave Passive Structures,* T. Itoh, Ed. New York: Wiley, 1989, ch. 8, pp. 496–591.

[4] P. B. Johns, "A symmetrical condensed node for the TLM-method," *IEEE Trans. Microwave Theory Tech.,* vol. MTT-35, no. 4, pp. 370–377, Apr. 1987.

[5] M. Krumpholz, P. Russer, and H. Zscheile, "The derivation of the condensed symmetric TLM node from Maxwell's equations," in *PIERS 1993,* Pasadena, CA, July 1993, p. 150.

[6] M. Krumpholz and P. Russer, "A field theoretical derivation of TLM," *IEEE Trans. Microwave Theory Tech.,* vol. 42, no. 9, pp. 1660–1886, Sept. 1994.

[7] P. Russer and M. Krumpholz, "On the field theoretical derivation of the transmission line matrix method," in *Second Int. Workshop on Discrete Time Domain Modelling of Electromagnetic Fields and Networks,* German IEEE MTT/AP joint chapter and CAS chapter, Berlin, Oct. 1993.

[8] H. Jin, R. Vahldieck, and J. Huang, "Direct derivation of the TLM symmetrical condensed node from Maxwell's equations using centered differencing and averaging," in *IEEE MTT-S Digest,* San Diego, CA, May 1994, pp. 23–26.

[9] W. J. R. Hoefer, "The discrete time domain Green's function or John's matrix—A new powerful concept in transmission line modelling," *Int. J. Numerical Modelling: Electronic Networks, Devices and Fields,* vol. 2, pp. 215–225, 1989.

[10] P. B. Johns and S. Akhtarzad, "The use of time-domain diacoptics in time discrete models of fields," *Int. J. Numer. Methods Eng.,* vol. 17, pp. 1–14, 1981.

[11] J. S. Nielsen, "TLM analysis of microwave and millimeter wave structures with embedded nonlinear devices," Ph.D. dissertation, University of Ottawa, 1992.

[12] J. S. Nielsen and W. J. R. Hoefer, "A complete dispersion analysis of the condensed node TLM mesh," *IEEE Trans. Magn.*, vol. 27, no. 5, pp. 3982–3985, Sept. 1991.
[13] M. Krumpholz and P. Russer, "On the dispersion in TLM and FDTD," *IEEE Trans. Microwave Theory Tech.*, vol. 42, no. 7, pp. 1275–1278, July 1994.
[14] ——, "Discrete time-domain Green's functions for three-dimensional TLM modelling of the radiating boundary conditions," in *ACES 1993*, Monterey, CA, Mar. 1993, pp. 458–466.
[15] P. Russer and M. Krumpholz, "The Hilbert space formulation of the TLM method," *Int. J. Numerical Modelling: Electronic Networks, Devices and Fields*, vol. 6, pp. 29–45, Feb. 1993.
[16] I. S. Gradshteyn and I. M. Ryzhik, *Table of Integrals, Series and Products*, 4th ed. New York: Academic, 1980, p. 1144.
[17] B. Engquist and A. Majda, "Absorbing boundary conditions for the numerical solution of waves," *Mathematics Comp.*, vol. 31, no. 139, pp. 629–651, July 1977.
[18] R. A. Renaut, "Absorbing boundary conditions, difference operators, and stability," *J. Comp. Phys.*, vol. 102, pp. 236–251, 1992.
[19] T. G. Moore, J. G. Blaschak, A. Taflove, and G. A. Kriegsmann, "Theory and application of radiation boundary operators," *IEEE Trans. Antennas Propagat.*, vol. AP-36, no. 12, pp. 1797–1812, Dec. 1988.
[20] J. A. Morente, J. A. Porti, and M. Khalladi, "Absorbing boundary conditions for the TLM method," *IEEE Trans. Microwave Theory Tech.*, vol. 40, pp. 2095–2099, Nov. 1992.
[21] C. Eswarappa and W. J. R. Hoefer, "Performance study of one-way absorbing boundary equations in 3-D TLM for dispersive guiding structures," in *IEEE MTT-S Dig.*, Atlanta, GA, June 1993, pp. 1439–1442.
[22] Z. Chen, M. M. Ney, and W. J. R. Hoefer, "Absorbing and connecting boundary conditions for the TLM method," *IEEE Trans. Microwave Theory Tech.*, vol. 41, no. 11, pp. 2016–2024, Nov. 1993.
[23] P. Saguet, "The 3D transmission-line matrix method: Theory and comparison of the processes," *Int. J. Numerical Modelling: Electronic Networks, Devices and Fields*, vol. 2, pp. 191–201, 1989.
[24] I. S. Gradshteyn and I. M. Ryzhik, *Table of Integrals, Series and Products*, 4th ed. New York: Academic, no. 2, sec. 3.915, 1980, p. 482.
[25] ——, *Table of Integrals, Series and Products*, 4th ed. New York: Academic, no. 14, sec. 6.561, 1980, p. 684.
[26] ——, *Table of Integrals, Series and Products*, 4th ed. New York: Academic, no. 2, sec. 3.723, 1980, p. 406.
[27] A. P. Prudnikov, Yu. A. Brychkow, and O. I. Mariakev, *Integrals and Series*. New York: Gordon and Breach, vol. 1, sec. 2.5.31, no. 7, 1986, p. 446.
[28] ——, *Integrals and Series*. New York: Gordon and Breach, vol. 2, no. 5, sec. 2.12.4, 1986, p. 177.
[29] ——, *Integrals and Series*. New York: Gordon and Breach, no. 17, sec. 2.12.4, 1986, p. 178.
[30] I. S. Gradshteyn and I. M. Ryzhik, *Table of Integrals, Series and Products*, 4th ed. New York: Academic, no. 3, sec. 3.723, 1980, p. 406.
[31] A. P. Prudnikov, Yu. A. Brychkow, and O. I. Mariakev, *Integrals and Series*. New York: Gordon and Breach, vol. 1, no. 6, sec. 2.5.31, 1986, p. 446.

Michael Krumpholz (M'94) was born in Bonn, Germany, in 1966. He received the Dipl.-Ing. degree and the Dr.-Ing. degree in electrical engineering at the Technische Universität München in 1991 and 1994, respectively.

From 1991 to 1992, he worked as a Research Assistant at the Lehrstuhl für Hochfrequenztechnik, Technische Universität München. In 1992, he joined the Ferdinand-Braun-Institut für Höchstfrequenztechnik Berlin. Since October 1994, he has been working as a Research Scientist at the Radiation Laboratory of the University of Michigan in Ann Arbor. His research interests are numerical methods for the solution of Maxwell's equations.

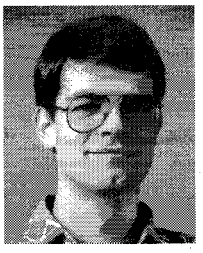

Bernhard Bader (S'91) was born in Betzigau, Germany, in 1966. He received the Dipl.-Ing. degree in 1992 from the Technische Universität in München, Germany.

In 1993 he joined the Ferdinand-Braun-Institut für Höchstfrequenztechnik in Berlin, Germany. Since that time, he has been engaged in research on computer-aided design methods for mircrowave circuits.

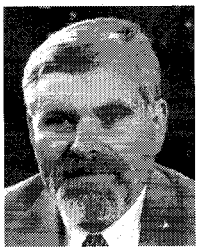

Peter Russer (SM'81–F'94) was born in Vienna, Austria, in 1943. He received the Dipl.-Ing. degree in 1967 and the Dr. techn. degree in 1971, both in electrical engineering, from the Technische Universität in Vienna, Austria.

From 1968 to 1971, he was an Assistant Professor at the Technische Universität in Vienna. In 1971 he joined the Research Institute of AEG-Telefunken in Ulm, where he worked on fiber-optic communication, broadband and low-noise solid-state electronic circuits, statistical noise analysis of microwave circuits, laser modulation, and fiber-optic gyroscopes. Since 1981 he has held the chair of Hochfrequenztechnik at the Technische Universität München. Since October 1992 he has also been Director of the Ferdinand-Braun-Institut für Höchstfrequenztechnik in Berlin. His current research interests are integrated microwave and millimeterwave circuits, electromagnetic fields, and methods for computer aided design of microwave circuits. He is the author of numerous scientific papers in these areas.

Dr. Russer is a member of the German Informationstechnische Gesellschaft and the Austrian and German Physical Societies. In 1979, he was corecipient of the NTG award.